

D-LIO: 6DoF Direct LiDAR-Inertial Odometry based on Simultaneous Truncated Distance Field Mapping

L. Coto-Elena¹, J.E. Maese¹, L. Merino¹ and F. Caballero¹

Abstract—This paper presents a new approach for 6DoF Direct LiDAR-Inertial Odometry (D-LIO) based on the simultaneous mapping of truncated distance fields on CPU. Such continuous representation (in the vicinity of the points) enables working with raw 3D LiDAR data online, avoiding the need of LiDAR feature selection and tracking, simplifying the odometry pipeline and easily generalizing to many scenarios. The method is based on the proposed Fast Truncated Distance Field (Fast-TDF) method as a convenient tool to represent the environment. Such representation enables i) solving the LiDAR point-cloud registration as a nonlinear optimization process without the need of selecting/tracking LiDAR features in the input data, ii) simultaneously producing an accurate truncated distance field map of the environment, and iii) updating such map at constant time independently of its size. The approach is tested using open datasets, aerial and ground. It is also benchmarked against other state-of-the-art odometry approaches, demonstrating the same or better level of accuracy with the added value of an online-generated TDF representation of the environment, that can be used for other robotics tasks as planning or collision avoidance. The source code is publicly available at <https://anonymous.4open.science/r/D-LIO>

I. INTRODUCTION

Accurate vehicle localization is a crucial aspect of robotics, directly influencing autonomous navigation, remote exploration, and other advanced applications. Various techniques are employed to improve localization, combining data from different sensors such as cameras, inertial measurement units (IMUs), LiDAR and radar [1]. LiDAR-based approaches [2] are widely used due to their capacity to provide high-density and accurate 3D data unaffected by lighting conditions. These techniques have been proven to provide accurate positioning while also enabling environmental mapping [3] [4]. However, they have certain limitations. In feature-sparse environments, traditional feature-based techniques [5] [6] may struggle to extract reliable information, leading to suboptimal localization. Additionally, when dealing with extremely dense point clouds, the computational cost increases significantly, making real-time execution challenging.

Beyond the choice of sensors, the underlying map representation plays a pivotal role in the accuracy and efficiency of localization systems. Most of the state-of-the-art LiDAR SLAM approaches represent maps in the form of point clouds

(3D points and/or features) together with ICP-like methods for LiDAR registration [7] [2]. While effective, these discrete representations often face challenges in scalability, sparsity, and differentiability [8] [9]. To address these limitations, distance fields, particularly Signed and Truncated Distance Fields [10], have emerged as a promising alternative. These volumetric representations capture obstacle proximity in a continuous fashion, which is especially beneficial for point cloud registration tasks by providing smooth gradients and implicit surface descriptions. However, the application to LiDAR SLAM is still limited to relatively small volumes (rooms, house floor, etc) or with large quantization errors that prevent their use in general purpose application [11] [12]. As a result, most LiDAR Distance Field approaches in the state of the art focus on mapping, assuming perfect sensor localization [13] [8].

This paper presents, to the best of our knowledge, the first 6DoF LiDAR Inertial SLAM method based on simultaneous mapping of truncated distance field in large volumes. Although the approach has potential for parallelization, it is able to map the environment and estimate the odometry approaching real time using just CPU. Unlike learning-based methods, the proposed Fast-TDF approach provides an accurate representation of the environment from the first scan.

The paper is structured as follows. First, Section II analyses the current state of the art on LiDAR odometry and distance field computation. Later, the proposed Fast Truncated Distance Field method is presented in Section III. Then, Section IV details the LiDAR-Inertial odometry approach based on simultaneous TDF mapping. The proposed methods are tested and benchmarked using public datasets and open-sourced LiDAR odometry approaches in Section V. Finally, Section VI presents the conclusions and future work.

II. STATE OF THE ART

A. LiDAR-based Odometry

Modern LiDAR-based odometry relies on high-resolution 3D point clouds to estimate motion, offering a key advantage over cameras by operating independently of ambient lighting conditions. Traditional methods, such as ICP [14] and NDT [15] register consecutive scans by minimizing alignment errors. These have been enhanced by approaches like GICP [7], CT-ICP [16] and KISS-ICP [2] that improve robustness and computational efficiency. Additionally, scan-to-map strategies, including IMLS-SLAM [17] and DLO [4], leverage accumulated map information to enhance localization stability.

*This work is partially supported by the grants INSERTION (PID2021-127648OB-C31) and NORDIC (TED2021-132476B-I00), both funded by the “Agencia Estatal de Investigación – Ministerio de Ciencia, Innovación y Universidades” and the “European Union NextGenerationEU/PRTR”.

¹The authors are with the Service Robotics Laboratory, Universidad Pablo de Olavide, Seville, Spain. {lcotele, jemaalv, lmercab, fcaballero}@upo.es

To reduce computational cost, feature-based methods extract geometric structures rather than using entire point clouds. LOAM [3] pioneered this approach by detecting edges and planar features, later extended by LeGO-LOAM [5] and by SuMa++ [18], which integrate segmentation and semantic constraints. Other methods, such as F-LOAM [6], further optimize the selection and representation of features for robust odometry.

Deep learning-based odometry has emerged to address challenges in feature consistency and matching. LO-Net [19] improves scan alignment by predicting surface normals and enforcing geometric constraints, while LodoNet [20] uses keypoint-based pose estimation. Unsupervised learning techniques, such as VertexNet [21], model pose uncertainty to enhance accuracy across diverse environments. These methods aim to improve generalization and robustness, complementing traditional LiDAR techniques.

Despite its advantages, LiDAR-only odometry faces several limitations. In featureless environments, such as tunnels, point cloud registration becomes unreliable due to insufficient constraints. Additionally, LiDAR's low frame rate (10–20 Hz) makes it less effective for capturing rapid motion dynamics. To mitigate these issues, sensor fusion with complementary modalities is employed to enhance robustness and computational efficiency. LiDAR-inertial odometry is an approach commonly used as IMU provide high-frequency inertial measurements capturing short-term motion dynamics with minimal latency.

Sensor fusion methods can be categorized depending on how each sensor contributes to the estimation of the pose. In loosely coupled approaches, LiDAR and IMU measurements are processed independently, and their outputs are fused at a later stage. These methods offer modularity and robustness but may not fully exploit the complementary nature of both sensors. Examples include LOAM [3] or Lego-LOAM [5].

On the other hand, tightly coupled approaches directly integrate raw IMU and LiDAR measurements within the same optimization framework, enabling continuous state estimation and higher accuracy. Methods such as LIO-SAM [1] or Faster-LIO [22] perform well in feature-sparse environments, where IMU constraints help maintain reliable pose estimates.

Despite advances in LiDAR-based odometry, several challenges still hinder its performance. One of the main issues is the high computational cost of processing dense point clouds, making it difficult to execute registration and optimization algorithms efficiently on hardware-constrained platforms. Another significant challenge is the difficulty of extracting discriminative features in homogeneous environments or repetitive geometries, potentially leading to errors in motion estimation. In such scenarios, direct odometry methods, that leverage the full point cloud information without relying on feature extraction, are often considered as an alternative [4] [18]. Furthermore, filtering and data reduction strategies must balance the need to decrease computational load while preserving essential information for localization.

B. Distance Fields Computation

Volumetric mapping and Simultaneous Localization and Mapping (SLAM) methods have significantly contributed to robot navigation, planning, and localization across diverse environments. These approaches primarily utilize discrete voxel-based structures, hierarchical data representations, probabilistic models, and implicit neural representations.

Voxel-based methods are extensively used due to their simplicity and ease of implementation. Voxblox [23] efficiently generates Euclidean Signed Distance Fields (ESDF) from Truncated Signed Distance Fields (TSDF), establishing a common baseline in volumetric mapping. FIESTA [24] further enhances computational efficiency by employing occupancy-based wavefront propagation instead of TSDF, thereby reducing complexity. Additionally, Voxfield [8] refines accuracy through non-projective TSDF fusion complemented by normal estimation from input point-cloud data. Despite their popularity and CPU efficiency, these voxel-based solutions exhibit inherent limitations such as scalability issues and discretization errors, reducing their effectiveness and precision in real-time SLAM applications.

Hierarchical data structures such as OpenVDB [9] have been proposed to mitigate scalability constraints. Approaches leveraging OpenVDB include VDB-EDT [25], which represents ESDF through efficient distance transforms. While these hierarchical methods improve scalability and memory usage, their discrete nature still limits smooth interpolation capabilities and continuous optimization.

Implicit neural representations have emerged as continuous alternatives to discrete methods, providing dense and differentiable volumetric maps. DeepSDF [26] introduced a neural-network-based implicit model to represent continuous SDFs. Continual Neural Mapping [27] proposed an incremental neural method employing replay buffers, but real-time incremental updates were first effectively demonstrated by iSDF [11]. More recently, HIO-SDF [12] introduced a hierarchical approach combining global voxel structures with local LiDAR data to train neural models online. TNDF-Fusion [28] compresses city-scale LiDAR maps via a Tri-Pyramid TNDF and NeRF-SLAM [29] delivers real-time dense monocular SLAM with hierarchical NeRFs, yet none of them unifies full 6-DoF LiDAR-inertial odometry with on-the-fly distance field mapping on a CPU. Despite these advances, neural methods typically require significant pre-training, heavy computation, and are limited to small-scale SLAM due to memory and inference constraints.

Gaussian Processes (GP) have been explored as probabilistic alternatives for representing distance fields, offering uncertainty estimation capabilities. Previous approaches have used GP-based models for uncertainty-aware mapping [30], but their inference remains computationally intensive due to the inversion of covariance matrices. To address computational constraints, hierarchical representations such as Octrees have been employed [30]. VDB-GPDF [13] leverages a logarithmic Gaussian Processes embedded within

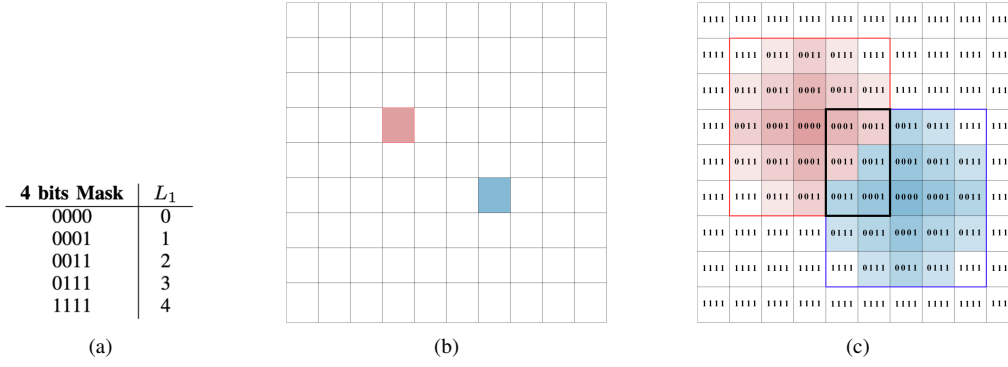


Fig. 1: 2D example of 5×5 binary kernel using 4 bits encoding. (a) Correspondence between mask and L_1 distance. (b) 2D occupancy representation of the input point cloud over the grid. (c) Merged distance map resulting from the bitwise-AND operation over overlapping binary kernels centered at each occupied cell.

the OpenVDB structure, generating continuous ESDFs with uncertainty measures. Nonetheless, the computational complexity associated with GP inference remains a significant obstacle for real-time implementation.

A significant limitation among these methodologies is their primary orientation toward mapping tasks, with limited or no direct application to real-time SLAM due to computational demands and quantization errors inherent in discretized representations. Consequently, real-time trajectory estimation and incremental map updates remain challenging.

In contrast, the approach proposed in this paper, Direct LiDAR Inertial Odometry (D-LIO), explicitly targets these limitations. D-LIO simplifies the odometry pipeline by eliminating the necessity for explicit LiDAR feature selection and tracking. Moreover, it maintains the environment map update process in constant time, irrespective of map size, significantly enhancing scalability. By directly fusing raw LiDAR point-cloud data into an optimized Fast Truncated Distance Field (Fast-TDF) representation, our method eliminates the additional computational overhead typically required to convert TSDF to ESDF, thus facilitating real-time integration into SLAM systems.

III. FAST TRUNCATED DISTANCE FIELD

Distance Fields (DFs) are able to provide the closest obstacle to a point in space, no matter how far we are from the obstacle. On the other hand, Truncated Distance Fields (TDFs) are only useful when the coordinate has an obstacle under its truncation distance. While this might be seen as a great advantage of DFs for localization, practical aspects limits and even dismiss such advantage because far points are normally rejected by the outlier rejection process during point cloud registration. Thus, if the truncation distance is properly tuned according to the localization approach at hand, TDFs might be a very efficient representation of the distance field.

This paper proposes using TDF to estimate the distance field. The proposed Fast-TDF takes advantage of binary masks to compute the L_1 distance into the area of influence of each obstacle. We will see how using binary masks to

encode TDFs is very convenient, changing the computational paradigm from map size dependence to point cloud size dependence, so that the computation will depend on the number of points to be included into the map, not the map size.

A. Binary kernel

Our Fast-TDF makes use of a binary kernel to compute the distance. This kernel must be applied to the map in each occupied cell. As a result, it will produce the distance of the surrounding free cells to the closest occupied under the truncation distance. The kernel represents the L_1 distance from each cell to an occupied cell in the center of the kernel. The distances into the kernel are expressed as bit-set masks following these conventions (Fig. 1.(a) shows an example of four bits):

- A zeroed mask indicates L_1 distance equal to zero.
- Starting with the Least Significant Bit (LSB), each bit set accounts for the distance between two consecutive cells.
- An all-one mask indicates the maximum L_1 distance, which is equal to the number of bits in the mask.

This distance encoding has a great advantage, we can compute the shortest distance into an arbitrary set by means of the bitwise-AND operation. No matter the number of distances or the values involved, a bitwise-AND among all the distances will provide the shortest value. This is positive at three levels: i) The bitwise-AND operation can be computed extremely fast in computers, with both, scalar and vectorized instructions, ii) We do not need to perform value comparisons at all, with the corresponding computation impact, and iii) The distance insertion order does not affect the result, because the bitwise-AND operation is commutative, which simplifies the parallelism.

As an illustrative example, let's assume we have three different distance values represented as a bit-set mask of 8 bits, these values are 00111111 ($L_1 = 6$), 00001111 ($L_1 = 4$) and 00000001 ($L_1 = 1$). The shortest distance among these

values can be easily computed by computing the bitwise-AND operation without performing value comparison:

$$00111111 \ \& \ 00001111 \ \& \ 00000001 = 00000001$$

Figure 1 illustrates a 2D example where two binary kernels of size 5×5 with 4 bit masks encoding are centered, respectively, on a red and a blue cell (Fig. 1.(b)). The bit mask encodes the L_1 distance, from 0000 at the kernel center ($L_1 = 0$) to 1111 at the corners ($L_1 = 4$), as shown in Fig. 1.(a). In Fig. 1.(c), both kernels are applied using bitwise-AND around their respective centers. In the overlapping region (outlined in black), we can see how the method preserves the shortest distance to the nearest center. All map cells were initialized to 1111 (the truncation distance) before applying the binary kernels, indicating the maximum or unknown distance.

B. TDF grid map

Notice that the previous kernel actually represents the L_1 TDF of an obstacle in its center. We can easily compute the TDF of a general point cloud as a grid map by just performing the bitwise-AND of this kernel with the grid map at each cell that contains a point. The representation of the distances in the form of a bit-set mask implicitly solves all the problems related to the distance field computation. Thus, we do not need to know if one point is close to any other, or the order of evaluation of points in the cloud.

Another advantage of this approach is its easy parallelization. In principle, each point can update the grid map in parallel, and then merge all updates by means of bitwise-AND. We can make use of this feature to accelerate the computation of the TDF, distributing the computation among different threads in the CPU.

Our TDF grid map will be represented as a 3D matrix of fixed resolution. The size of the grid is determined by the spatial distribution of 3D points. Every grid cell contains the L_1 distance to the closest point of the 3D map to that cell, or the truncation distance if the closest point is far.

The truncation distance will be defined by three factors: the number of bits used to represent the bit-set mask, the size of the kernel, and the grid resolution. The number of bits of the mask must be equal to the maximum L_1 distance into the kernel in order to make the approach efficient, so the truncation distance will be finally given by the size of the kernel and the resolution.

C. Grid map initialisation and access

As previously introduced, the grid map is a 3D matrix containing a binary mask for each cell in the space. The number of bits per cell will be defined by the binary mask size itself. As we have a dense representation of the world, it is not recommended to use sparse representations such as kd-trees [31] or Octomap [32]. Instead, we use a large memory array to represent the space at fixed resolution. A simple hash function is used to transform the 3D coordinates into the corresponding index in the array (see details in the

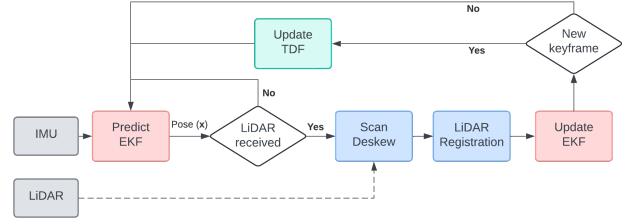


Fig. 2: D-LIO Workflow. Red indicates the Kalman filter, green the TDF grid map, and blue the LiDAR preprocessing and optimization.

source code). In this way, the time required for grid access is extremely small, and more importantly, constant.

Such grid map must be correctly initialized in order to properly work with the binary kernel bitwise-AND operation. Thus, the whole grid must be initialized to the truncation distance, that is, a mask with all bits set. This value will be updated by the binary kernel as soon as the value to store into the grid cell is smaller than the truncation distance.

D. Distance computation

The grid map stores binary masks, not distances. We need a method to compute the actual L_1 distance from the binary mask in the grid cells. We make use of the C++ `std::bitset()` standard function, which is directly mapped into computer assembly instructions. This function counts the number of bits set into a register, returning an integer with such number, the corresponding L_1 distance.

E. Distance interpolation

Following [33], we make use of trilinear interpolation in order to estimate the distance field beyond the grid cell resolution. Trilinear interpolation is used as a trade-off between computation and accuracy. Thus, tricubic interpolation offers better accuracy, however its computation load in each grid cell prevents its online use.

Using trilinear interpolation also offers an easy and quick distance field gradient approximation. Given such gradient approximation, we can analytically compute complex gradients with respect to third-party variables, as robot position or orientation for localization. Contrary to [33], this interpolation is computed online.

IV. DIRECT 3D LiDAR-INERTIAL ODOMETRY

Figure 2 shows a block diagram of the D-LIO approach. The algorithm incrementally estimates the system pose using an Extended Kalman Filter (EKF) by integrating inertial measurements for pose prediction and point cloud to map registration for pose update. Thus, for each incoming point cloud, the system performs a cloud registration by aligning it with the environment mapped so far based on the Truncated Distance Field (TDF), using the EKF estimate as initial guess. This alignment is used to constraint the EKF's pose and velocity by means of state update. Whenever the estimated pose variation exceeds a predefined threshold, the

TDF map is updated by incorporating new information. This updated map then facilitates a more precise alignment of subsequent point clouds during the registration process.

A. Inertial State Integration

Following LiDAR odometry common practices [34] [35], inertial sensors can be used to improve state estimation between scans. Inertial integration provides a good initial solution for LiDAR scan alignment, which benefits the subsequence scan-matching process. In addition, high-frequency inertial integration enables LiDAR scan deskewing, which also positively impacts the quality of the scan-matching process. We make use of an EKF with the following state vector:

$$\mathbf{x} = [\mathbf{p}, \mathbf{v}, \mathbf{a}_b, \mathbf{r}, \mathbf{g}_b]^t \quad (1)$$

where the state encapsulates the 3D position $\mathbf{p} = (x, y, z)$, linear velocity $\mathbf{v} = (v_x, v_y, v_z)$, accelerometer bias $\mathbf{a}_b = (a_{bx}, a_{by}, a_{bz})$, orientation $\mathbf{r} = (r_x, r_y, r_z)$ and gyroscope bias $\mathbf{g}_b = (g_{bx}, g_{by}, g_{bz})$. Here, the position \mathbf{p} , velocity \mathbf{v} , and orientation \mathbf{r} are expressed in the global frame, while the accelerometer and gyroscope biases, \mathbf{a}_b and \mathbf{g}_b respectively, are expressed in the local inertial frame.

In the prediction step, the filter integrates IMU measurements (angular velocity and linear acceleration) to propagate the state forward in time. Once a new LiDAR scan is received, deskewing is performed using the high-rate inertial state estimates to compensate for motion-induced distortions accumulated during the scan acquisition. Subsequently, the update step is carried out using the refined pose from the cloud registration step and the estimated velocity derived from successive point cloud positions.

B. LiDAR point-cloud registration

This point cloud registration is formulated as a nonlinear optimization problem over the SE(3) space, where the objective is to minimize the distance from each point to the closest object in the map. The point-cloud is pre-transformed according to the EKF current state, so that the registration only needs to deal with the accumulated error in the inertial integration between scans.

The problem is formulated as the following minimization of a sum of residuals:

$$\min_{\mathbf{t}, \mathbf{q}} \sum_i \rho_i L_1(\mathbf{R}(\mathbf{q}) \cdot \mathbf{p}_i + \mathbf{t})^2 \quad (2)$$

where i corresponds to each point in the cloud, $\mathbf{t} \in \mathbb{R}^3$ is the translation vector, $\mathbf{q} \in \mathbb{H}$ is the unit quaternion encoding rotation, $\mathbf{R}(\mathbf{q})$ is the corresponding rotation matrix, ρ_i is the robust kernel detailed in Section IV-C, and $L_1(\cdot)$ returns the unsigned L_1 distance to the nearest object using trilinear interpolation over the TDF computed so far as explained in Sections III-D and III-E.

The optimization is carried out using the Ceres Solver library [36]. To properly handle the unit norm constraint of quaternions, a proper Lie group formulation is applied, along with its corresponding Lie algebra, enabling optimization in the tangent space.

C. Outlier rejection

Before formulating the optimization problem, points that fall outside the TDF grid are discarded to ensure valid distance evaluations. For the remaining points, a robust loss function is applied to mitigate the effect of outliers while preserving global consistency in the estimation. In particular, a Cauchy loss is employed, whose scale parameter is a function of the point's distance to the sensor:

$$\rho_i = \text{CauchyLoss}(\lambda \cdot (0.1 + 0.1 \cdot \|\mathbf{p}_i\|)) \quad (3)$$

where λ is a tuning factor and $\|\mathbf{p}_i\|$ denotes the Euclidean norm of the 3D point \mathbf{p}_i expressed in the LiDAR sensor system reference.

This robust kernel ensures that distant points are not excessively penalized due to their higher residuals, which can naturally arise from small orientation errors. For example, a rotation error of just 1° may produce negligible displacements in nearby points (e.g., a few centimeters), but can lead to significant deviations (e.g., a few meters) in distant points. If a fixed-scale robust loss were used, these far points could be interpreted as outliers and ignored during optimization, causing the system to converge to a locally optimal but globally inaccurate solution. The proposed kernel preserves the contribution of both near and far points, promoting robust convergence across the entire cloud.

D. Key-framing and map updating

A keyframe-based approach is employed for map updates, where a new keyframe is created whenever the relative translation or rotation with respect to the previous keyframe exceeds the predefined thresholds t_{th} and q_{th} , respectively. When a new keyframe is created, the TDF map is updated by integrating the current point cloud, which is first transformed according to the latest optimized pose estimate, ensuring proper alignment in the global frame before fusion. This process, detailed in Section III, updates the TDF grid by performing bitwise-AND operations of the kernel centered at each point, integrating it from the transformed cloud into the grid while considering both the new point and the existing map data. Although it is the most computationally expensive stage of the system, the use of bitwise-AND operations and parallelization helps optimize the map update process and significantly reduce processing time.

V. EXPERIMENTAL RESULTS

The algorithm has been tested on two datasets, the **VIRAL Dataset** [37] and the **Newer College Dataset** [38], to evaluate its ability to correctly localize in different environments using diverse trajectories that challenge its performance.

The accurate estimation of odometry has been primarily validated with the VIRAL Dataset, as it features more challenging environments, including the presence of trees, reflective or transparent surfaces, and complex aerial trajectories that test the algorithm's stability. On the other hand, with the Newer College Dataset, the correct generation of a grid has been assessed in a significantly larger environment

in order to demonstrate the algorithm’s scalability concerning map size and number of points. A supplementary video presents qualitative results and 3D reconstructions.¹

In both datasets, the Absolute Translation Error (ATE) has been computed by comparing the estimated trajectory with the ground truth. We used the benchmarking tools provided by the VIRAL dataset to ensure a consistent and reliable trajectory evaluation.

The results obtained on both datasets are presented in Table I together with other approaches, such as A-LOAM [39], M-LOAM [40], FAST-LIO2 [35], KISS-ICP [2], and LIO-SAM [1]. The metrics of A-LOAM, M-LOAM, and LIO-SAM were taken from the VIRAL-SLAM paper [41], and those for KISS-ICP from [42]. The LIO-SAM results in **quad-easy** sequence are taken from NV-LIOM [43]. Please, notice that LIO-SAM performs back-end optimization, which makes the comparison with pure odometry not entirely fair. However, we have included its results to demonstrate that our approach, despite not using back-end optimization, achieves comparable performance. As shown in Table I, our method attains the lowest ATE in the majority of sequences and ranks second-best in the remainder, highlighting its consistent accuracy and robustness across diverse and challenging trajectories.

These experimental results made use of FastTDF configured with a $40 \times 40 \times 40$ binary kernel using 64 bit mask encoding. Together with a grid resolution of 0.05 m, the truncation distance of this kernel is approximately 3 meters.

A. VIRAL Dataset

Our algorithm has been tested on the sequences “eee”, “nya”, and “sbs”, each with three sub-trajectories. These sequences cover diverse environments, including indoor and enclosed spaces, open areas with varying building heights, and surfaces that challenge LiDAR odometry, such as glass and semi-transparent materials.

The vehicle employed to record this dataset is a DJI M600 Hexacopter equipped with several sensors, including the IMU “VectorNav VN100” and the horizontal and vertical LiDAR “Ouster OS1-16 gen 1”, with a combined point cloud density of approximately 20 k points per frame. For these experiments, the map size was set to $60 \times 60 \times 25$ meters, and the parameters $\lambda = 1.0$, $t_{th} = 2$ m, and $q_{th} = 25^\circ$.

Figure 3 shows the 3D reconstruction generated by D-LIO, along with the trajectory used to obtain it. More comprehensive results, including the estimated trajectories from all runs and their associated visualizations, will be made available in the corresponding GitHub repository².

B. Newer College Dataset

In this dataset, the “Quad-Easy” trajectory has been followed, which involves two loops in the quad area with a nominal walking speed. The platform is equipped with a series of sensors, of which we have only used the LiDAR “Ouster OS-0-128”, which already comes with an integrated

IMU, as the inertial information also comes from the IMU integrated into the LiDAR. In this case, the platform is manually carried by a person, who performs a couple of loops over the environment at a constant speed. For these experiments, the map size has been set to $80 \times 60 \times 35$ meters, and the parameters $\lambda = 1.0$, $t_{th} = 1$ m, and $q_{th} = 25^\circ$.

As shown in Figure 4, the trajectory followed is relatively simple, and the D-LIO successfully estimates a value comparable to those achieved by state-of-the-art methods listed in Table I. The particularity of this environment lies in both its large scale (approximately $80 \times 60 \times 35$ meters) and the high point density of the LiDAR sensor, around 100 k points per frame. The objective of testing this dataset is to observe the algorithm’s scalability in environments with high point densities, as existing algorithms using odometry with distance field generation struggle with such scalability.

C. Runtime and memory consumption

The experiments were performed on an HP Victus 16 laptop equipped with 32 GB RAM and a 13th generation Intel Core i7-13700H processor. No GPU was used for the experimentation. The performance of the system was analyzed in terms of memory usage, CPU load, and execution time for the two datasets analyzed, using the same configuration in both cases. Regarding memory consumption, the college dataset exhibits a footprint ranging from 30% to 90%, while in the VIRAL dataset, memory usage is generally lower, between 10% and 40%. In both cases, the grid update step is the primary contributor to memory usage.

Overall memory consumption is primarily determined by the size of the selected map, since a fixed portion of memory is reserved for the grid. Consequently, the experiments on the college dataset consumed around 19 GB of memory, while those on VIRAL, with a smaller map, required approximately 10 GB.

Execution times are summarized in Table II, reporting the average times measured over several trajectories without downsampling, thus reflecting the most demanding scenario. The map update step consistently emerges as the most computationally expensive stage, often becoming the bottleneck of the algorithm. This update time strongly depends on the density of the point cloud to be integrated. For instance, in the VIRAL dataset, the lower density of points from both the horizontal and vertical OS-1 (approx. 20 k points per scan) leads to shorter map update times (≈ 0.30 s), whereas in the college dataset, where the LiDAR produces around 100 k points/scan, the update step is significantly slower (≈ 1.2 s). However, the map update time has little impact on the average total time (see Table II) because our method performs the update operation at a much lower frequency than the sensor acquisition (10 Hz), while the optimization step, which is executed at every scan, remains lightweight (typically below 0.05 s). This design allows the overall average computation time per scan to remain below the LiDAR rate in most cases, except for the College dataset, where the high point density and frequent updates during longer motion intervals result in a higher total runtime.

¹<https://youtu.be/iIVCYR85AHg>

²<https://anonymous.4open.science/r/D-LIO>

TABLE I: Experimental results, ATE (m), on VIRAL and New College Dataset across different algorithms. The best result is highlighted in **bold** and the second best is underlined, excluding LIO-SAM as it performs back-end optimization.

	D-LIO	A-LOAM	M-LOAM	FAST-LIO2	KISS-ICP	LIO-SAM
eee01	0.092	0.212	0.249	<u>0.166</u>	2.383	0.075
eee02	0.083	0.199	0.168	<u>0.100</u>	1.586	0.069
eee03	0.122	0.148	0.233	<u>0.142</u>	1.055	0.101
nya01	<u>0.080</u>	0.077	0.123	0.127	0.359	0.076
nya02	<u>0.104</u>	0.091	0.191	0.151	-	0.07
nya03	0.065	<u>0.108</u>	0.226	0.130	1.389	0.137
sbs01	0.094	<u>0.103</u>	0.173	0.130	1.353	0.089
sbs02	0.061	<u>0.091</u>	0.147	0.144	1.435	0.083
sbs03	0.098	0.367	0.153	0.126	<u>1.037</u>	0.14
quad-easy	<u>0.093</u>	0.085	0.141	0.100	0.100	0.074

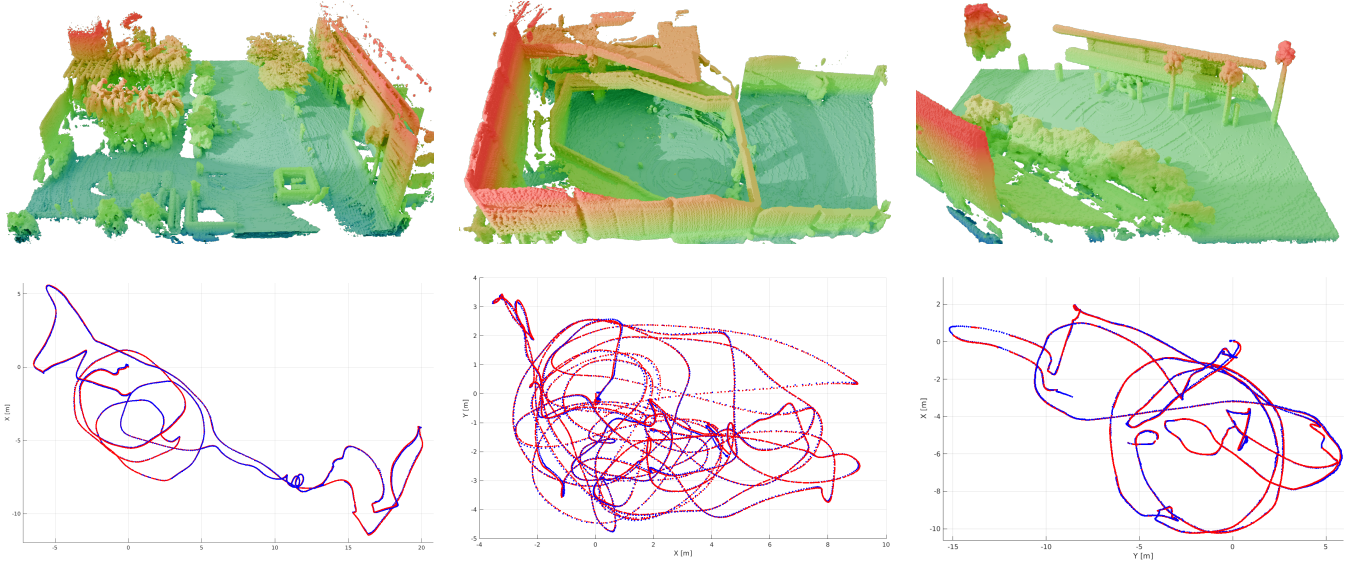


Fig. 3: 3D Map reconstruction of maps “eee”, “nya” and “sbs” alongside with each estimated 2D trajectory, where groundtruth is shown in red and the estimated trajectory in blue.

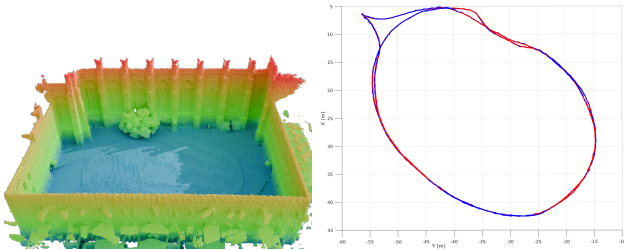


Fig. 4: 3D Map reconstruction of map “Quad-Easy” from Newer College Dataset alongside with estimated trajectory.

TABLE II: Runtime analysis across different datasets, showing mean \pm standard deviation (in seconds) for each processing phase.

Dataset	Total (s)	Optimize (s)	Update (s)
college	0.583 ± 0.433	0.430 ± 0.187	1.216 ± 0.060
eee	0.052 ± 0.051	0.040 ± 0.015	0.301 ± 0.036
nya	0.083 ± 0.071	0.065 ± 0.024	0.367 ± 0.022
sbs	0.051 ± 0.048	0.044 ± 0.016	0.301 ± 0.014

VI. CONCLUSIONS AND FUTURE WORK

It is also worth noting that state-of-the-art distance field mapping approaches, such as VDB-GPDF [13], which focuses solely on reconstruction, reported similar execution times to ours, but our approach performs both odometry and reconstruction without any downsampling. Although the map is updated less frequently, once every meter, it integrates the full-resolution point cloud, offering a balanced trade-off between computational efficiency and mapping accuracy.

D-LIO, a fully direct LiDAR–inertial odometry pipeline based on Fast-TDF simultaneous mapping, has been shown to match or outperform feature-driven state-of-the-art methods while producing a continuously available distance field for downstream tasks. Unlike conventional TSDF/ESDF frameworks whose update cost grows with map volume, our Fast-TDF binary-mask scheme ties each integration step solely to the number of incoming points. By encoding obstacle proximity directly in the truncated distance field, we avoid feature extraction, yielding robust convergence even in feature-sparse or highly reflective environments. The

resulting TDF is immediately usable for collision avoidance or planning without any post-processing.

Future work will focus on two main extensions. First, addressing the limitation of using a fixed-size grid, as there is currently no strategy to manage the map when the system approaches its spatial limits. Introducing dynamic resizing or shifting methods could improve scalability in larger environments. Second, extending the Fast-TDF kernel to support signed distance estimation, enabling the system to distinguish whether a point lies in front of or behind an obstacle, potentially enhancing registration accuracy.

REFERENCES

- [1] T. Shan, B. Englot, D. Meyers, W. Wang, C. Ratti, and R. Daniela, "Lio-sam: Tightly-coupled lidar inertial odometry via smoothing and mapping," in *IEEE/RSJ International Conference on Intelligent Robots and Systems (IROS)*. IEEE, 2020, pp. 5135–5142.
- [2] I. Vizzo, T. Guadagnino, B. Mersch, L. Wiesmann, J. Behley, and C. Stachniss, "Kiss-icp: In defense of point-to-point icp simple, accurate, and robust registration if done the right way," *IEEE Robotics and Automation Letters*, vol. PP, pp. 1–8, 02 2023.
- [3] J. Zhang and S. Singh, "Loam : Lidar odometry and mapping in real-time," *Robotics: Science and Systems Conference (RSS)*, pp. 109–111, 01 2014.
- [4] K. Chen, B. T. Lopez, A.-a. Agha-mohammadi, and A. Mehta, "Direct lidar odometry: Fast localization with dense point clouds," *IEEE Robotics and Automation Letters*, vol. 7, no. 2, pp. 2000–2007, 2022.
- [5] T. Shan and B. Englot, "Lego-loam: Lightweight and ground-optimized lidar odometry and mapping on variable terrain," 10 2018, pp. 4758–4765.
- [6] H. Wang, C. Wang, C.-L. Chen, and L. Xie, "F-loam : Fast lidar odometry and mapping," in *2021 IEEE/RSJ International Conference on Intelligent Robots and Systems (IROS)*, 2021, pp. 4390–4396.
- [7] A. Segal, D. Hähnel, and S. Thrun, "Generalized-icp," 06 2009.
- [8] Y. Pan, Y. Kompis, L. Bartolomei, R. Mascaro, C. Stachniss, and M. Chli, "Voxfield: Non-projective signed distance fields for online planning and 3d reconstruction," in *2022 IEEE/RSJ International Conference on Intelligent Robots and Systems (IROS)*, 2022, pp. 5331–5338.
- [9] K. Museth, "Vdb: High-resolution sparse volumes with dynamic topology," *ACM Trans. Graph.*, vol. 32, pp. 27:1–27:22, 07 2013.
- [10] B. Curless and M. Levoy, "A Volumetric Method for Building Complex Models From Range Images," in *Proceedings of the 23rd Annual Conference on Computer Graphics and Interactive Techniques - SIGGRAPH '96*. ACM Press, 1996.
- [11] J. Ortiz, A. Clegg, J. Dong, E. Sucar, D. Novotny, M. Zollhoefer, and M. Mukadam, "isdf: Real-time neural signed distance fields for robot perception," 2022. [Online]. Available: <https://arxiv.org/abs/2204.02296>
- [12] V. Vasilopoulos, S. Garg, J. Huh, B. Lee, and V. Isler, "Hio-sdf: Hierarchical incremental online signed distance fields," 2024. [Online]. Available: <https://arxiv.org/abs/2310.09463>
- [13] L. Wu, C. L. Gentil, and T. Vidal-Calleja, "Vdb-gpdf: Online gaussian process distance field with vdb structure," 2024. [Online]. Available: <https://arxiv.org/abs/2407.09649>
- [14] P. Besl and N. D. McKay, "A method for registration of 3-d shapes," *IEEE Transactions on Pattern Analysis and Machine Intelligence*, vol. 14, no. 2, pp. 239–256, 1992.
- [15] P. Biber and W. Strasser, "The normal distributions transform: a new approach to laser scan matching," in *Proceedings 2003 IEEE/RSJ International Conference on Intelligent Robots and Systems (IROS 2003) (Cat. No.03CH37453)*, vol. 3, 2003, pp. 2743–2748 vol.3.
- [16] P. Dellenbach, J.-E. Deschaud, B. Jacquet, and F. Goulette, "Ct-icp: Real-time elastic lidar odometry with loop closure," in *2022 International Conference on Robotics and Automation (ICRA)*, 2022, pp. 5580–5586.
- [17] J.-E. Deschaud, "Imls-slam: Scan-to-model matching based on 3d data," in *2018 IEEE International Conference on Robotics and Automation (ICRA)*, 2018, pp. 2480–2485.
- [18] X. Chen, A. Milioto, E. Palazzolo, P. Giguère, J. Behley, and C. Stachniss, "Suma++: Efficient lidar-based semantic slam," 11 2019, pp. 4530–4537.
- [19] Q. Li, C. Shaoyang, C. Wang, X. Li, C. Wen, M. Cheng, and J. Li, "Lo-net: Deep real-time lidar odometry," 06 2019, pp. 8465–8474.
- [20] C. Zheng, Y. Lyu, M. Li, and Z. Zhang, "Lodonet: A deep neural network with 2d keypoint matching for 3d lidar odometry estimation," in *Proceedings of the 28th ACM International Conference on Multimedia*, ser. MM '20. ACM, Oct. 2020, p. 2391–2399. [Online]. Available: <http://dx.doi.org/10.1145/3394171.3413771>
- [21] Y. Cho, G. Kim, and A. Kim, "Unsupervised geometry-aware deep lidar odometry," in *2020 IEEE International Conference on Robotics and Automation (ICRA)*, 2020, pp. 2145–2152.
- [22] C. Bai, T. Xiao, Y. Chen, H. Wang, F. Zhang, and X. Gao, "Faster-lio: Lightweight tightly coupled lidar-inertial odometry using parallel sparse incremental voxels," *IEEE Robotics and Automation Letters*, vol. 7, pp. 4861–4868, 04 2022.
- [23] H. Oleynikova, Z. Taylor, M. Fehr, R. Siegwart, and J. Nieto, "Voxblox: Incremental 3d euclidean signed distance fields for on-board mav planning," in *2017 IEEE/RSJ International Conference on Intelligent Robots and Systems (IROS)*. IEEE, sep 2017, p. 1366–1373. [Online]. Available: <http://dx.doi.org/10.1109/IROS.2017.8202315>
- [24] L. Han, F. Gao, B. Zhou, and S. Shen, "Fiesta: Fast incremental euclidean distance fields for online motion planning of aerial robots," 2019. [Online]. Available: <https://arxiv.org/abs/1903.02144>
- [25] D. Zhu, C. Wang, W. Wang, R. Garg, S. Scherer, and M. Q. H. Meng, "Vdb-edt: An efficient euclidean distance transform algorithm based on vdb data structure," 2021. [Online]. Available: <https://arxiv.org/abs/2105.04419>
- [26] J. J. Park, P. Florence, J. Straub, R. Newcombe, and S. Lovegrove, "Deepsdf: Learning continuous signed distance functions for shape representation," 2019. [Online]. Available: <https://arxiv.org/abs/1901.05103>
- [27] Z. Yan, Y. Tian, X. Shi, P. Guo, P. Wang, and H. Zha, "Continual neural mapping: Learning an implicit scene representation from sequential observations," 2021. [Online]. Available: <https://arxiv.org/abs/2108.05851>
- [28] Z. Chen, K. Zhang, H. Chen, M. Y. Wang, W. Zhang, and H. Yu, "Tndf-fusion: Implicit truncated neural distance field for lidar dense mapping and localization in large urban environments," *IEEE Robotics and Automation Letters*, vol. 9, no. 9, pp. 7445–7452, 2024.
- [29] A. Rosinol, J. J. Leonard, and L. Carlone, "Nerf-slam: Real-time dense monocular slam with neural radiance fields," 2022. [Online]. Available: <https://arxiv.org/abs/2210.13641>
- [30] C. L. Gentil, O.-L. Ouabi, L. Wu, C. Pradalier, and T. Vidal-Calleja, "Accurate gaussian-process-based distance fields with applications to echolocation and mapping," 2023. [Online]. Available: <https://arxiv.org/abs/2302.13005>
- [31] M. Skrodzki, "The k-d tree data structure and a proof for neighborhood computation in expected logarithmic time," 2019. [Online]. Available: <https://arxiv.org/abs/1903.04936>
- [32] K. Wurm, A. Hornung, M. Bennewitz, C. Stachniss, and W. Burgard, "Octomap: A probabilistic, flexible, and compact 3d map representation for robotic systems," vol. 2, 01 2010.
- [33] F. Caballero and L. Merino, "DLL: Direct LIDAR Localization. A map-based localization approach for aerial robots," in *IEEE/RSJ International Conference on Intelligent Robots and Systems*, 2021.
- [34] Y. Wu, T. Guadagnino, L. Wiesmann, L. Klingbeil, C. Stachniss, and H. Kuhlmann, "Lio-ekf: High frequency lidar-inertial odometry using extended kalman filters," in *2024 IEEE International Conference on Robotics and Automation (ICRA)*, 2024, pp. 13 741–13 747.
- [35] W. Xu, Y. Cai, D. He, J. Lin, and F. Zhang, "Fast-lio2: Fast direct lidar-inertial odometry," 2021. [Online]. Available: <https://arxiv.org/abs/2107.06829>
- [36] S. Agarwal, K. Mierle, and T. C. S. Team, "Ceres Solver," 10 2023. [Online]. Available: <https://github.com/ceres-solver/ceres-solver>
- [37] T.-M. Nguyen, S. Yuan, M. Cao, Y. Lyu, T. H. Nguyen, and L. Xie, "Ntu viral: A visual-inertial-ranging-lidar dataset, from an aerial vehicle viewpoint," *The International Journal of Robotics Research*, vol. 41, no. 3, pp. 270–280, 2022.
- [38] L. Zhang, M. Camurri, D. Wisth, and M. Fallon, "Multi-camera lidar inertial extension to the newer college dataset," 2021.
- [39] T. Wang, X. Wu, H. Yang, P. Zhao, and Q. Hu, "An improved a-loam 3d mapping method based on ultra-wide field angle of multi-line lidar," in *2022 29th International Conference on Geoinformatics*, 2022, pp. 1–6.

- [40] J. Jiao, H. Ye, Y. Zhu, and M. Liu, "Robust odometry and mapping for multi-lidar systems with online extrinsic calibration," *IEEE Transactions on Robotics*, vol. PP, pp. 1–10, 05 2021.
- [41] "Viral slam: Tightly coupled camera-imu-uwblidar slam," 05 2021.
- [42] J. L. Blanco-Claraco, "A flexible framework for accurate lidar odometry, map manipulation, and localization," 2024. [Online]. Available: <https://arxiv.org/abs/2407.20465>
- [43] D. Chung and J. Kim, "Nv-liom: Lidar-inertial odometry and mapping using normal vectors towards robust slam in multifloor environments," *IEEE Robotics and Automation Letters*, vol. 9, no. 11, pp. 9375–9382, 2024.